AD-A038 874 GEORGIA INST OF TECH ATLANTA SCHOOL OF AEROSPACE ENG--ETC F/G 20/4
EXPERIMENTS AND ANALYSIS RELATED TO EXTERNAL BURNING FOR PROPUL--ETC(U)
MAR 77 D H NEALE, J E HUBBARTT, W C STRAHLE AF-AFOSR-2794-75
UNCLASSIFIED AFOSR-TR-77-0602 NL

| OF |
AD
A038874

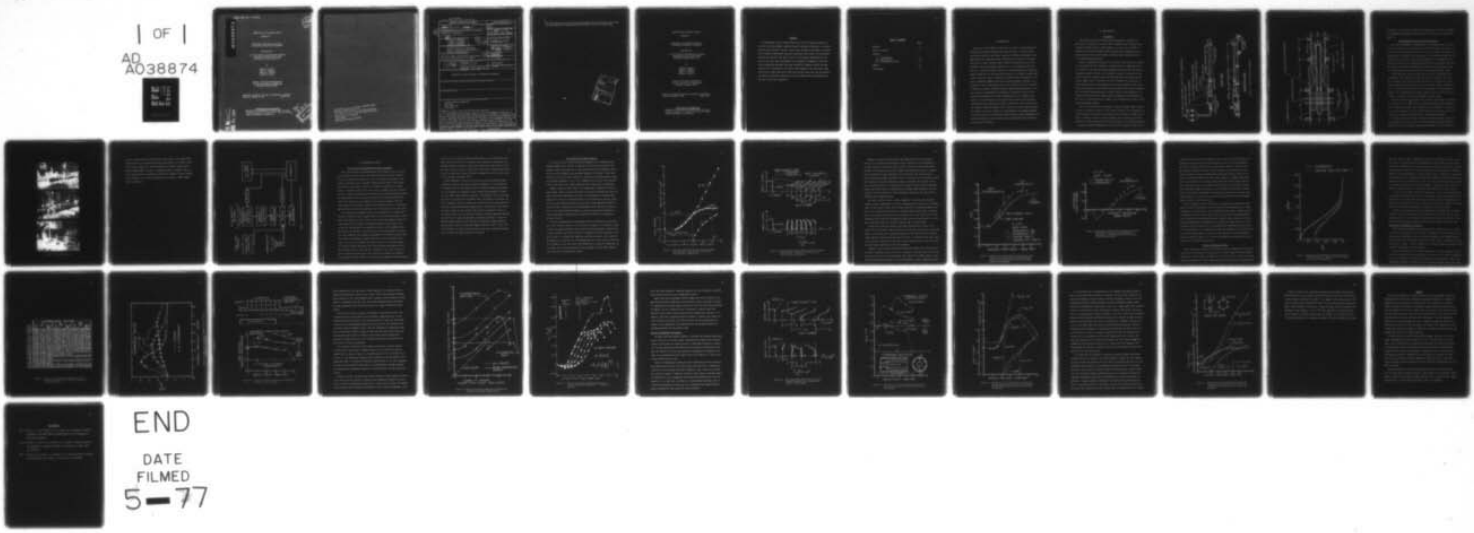

END

DATE
FILMED
5-77

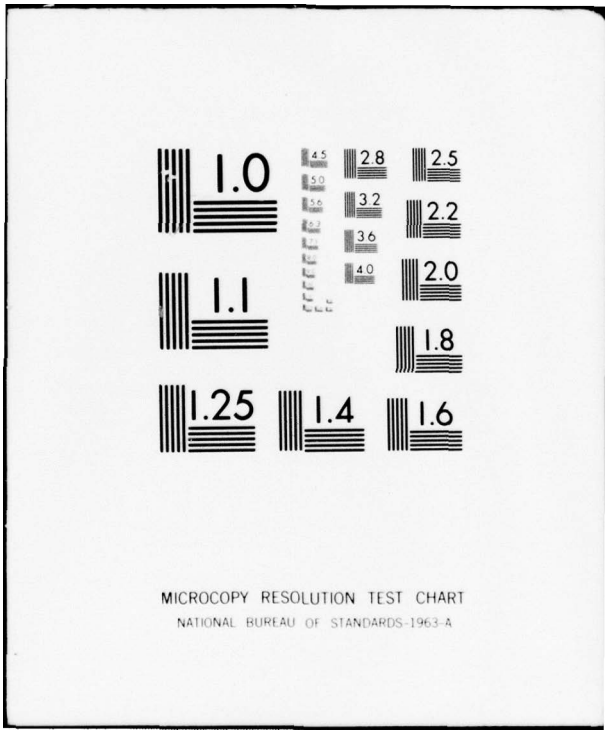
1.0
1.1
1.25
1.4
1.6
1.8
2.0
2.2
2.5
2.8
3.2
3.6
4.0
4.5
5.0
5.6
MICROCOPY RESOLUTION TEST CHART
NATIONAL BUREAU OF STANDARDS-1963-A

12 NW

AFOSR Interim Scientific Report

AFOSR-TR-

Experiments and Analysis Related to External Burning for Propulsion

Prepared for

Air Force Office of Scientific Research
Aerospace Sciences Directorate
Bolling Air Force Base, D. C.

by

Douglas H. Neale
James E. Hubbartt
Warren C. Strahle
Walter W. Wilson

School of Aerospace Engineering
Georgia Institute of Technology
Atlanta, Georgia 30332

Approved for public release; distribution unlimited
Grant No. AFOSR 75-2794 March 1977

AIR FORCE OFFICE OF SCIENTIFIC RESEARCH (AFSC)
NOTICE OF TRANSMITTAL TO DDC
This technical report has been reviewed and is
approved for public release IAW AFR 190-12 (7b).
Distribution is unlimited.
A. D. BLOSE
Technical Information Officer

Unclassified

SECURITY CLASSIFICATION OF THIS PAGE (When Data Entered)

REPORT DOCUMENTATION PAGE

READ INSTRUCTIONS BEFORE COMPLETING FORM

1. REPORT NUMBER: AFOSR-TR-77-0602

2. GOVT ACCESSION NO.

3. RECIPIENT'S CATALOG NUMBER

4. TITLE (and Subtitle): Experiments and Analysis Related to External Burning for Propulsion

5. TYPE OF REPORT & PERIOD COVERED: INTERIM rept. Feb 1976 - Jan 1977

6. PERFORMING ORG. REPORT NUMBER

7. AUTHOR(s): Douglas H. Neale, James E. Hubbartt, Warren C. Strahle, Walter W. Wilson

8. CONTRACT OR GRANT NUMBER(s): AF AFOSR-75-2794-75

9. PERFORMING ORGANIZATION NAME AND ADDRESS:
Georgia Institute of Technology
School of Aerospace Engineering
Atlanta, Georgia 30332

10. PROGRAM ELEMENT, PROJECT, TASK AREA & WORK UNIT NUMBERS: 2308/A2, 61102F, A2

11. CONTROLLING OFFICE NAME AND ADDRESS:
Air Force Office of Scientific Research/NA
Bolling Air Force Base, D. C. 20332

12. REPORT DATE: March 1977

13. NUMBER OF PAGES: 34

14. MONITORING AGENCY NAME & ADDRESS (if different from Controlling Office): 44p. AFOSR TR-77-0602

15. SECURITY CLASS. (of this report): Unclassified

15a. DECLASSIFICATION/DOWNGRADING SCHEDULE

16. DISTRIBUTION STATEMENT (of this Report)

Approved for public release; distribution unlimited

17. DISTRIBUTION STATEMENT (of the abstract entered in Block 20, if different from Report)

18. SUPPLEMENTARY NOTES

19. KEY WORDS (Continue on reverse side if necessary and identify by block number)

External burning propulsion
Base flow
Supersonic flow
Wind tunnel

20. ABSTRACT (Continue on reverse side if necessary and identify by block number)

An experimental study of base flow for a 2.25 inch diameter projectile at Mach 3 with and without simulated external burning disturbances is reported. Base pressure and wake structure results from systematic variations in axisymmetric external compression show that substantial base thrust can be produced and that the pressure and length scales of the external compression are imposed on the near wake. Measurements with comparable axisymmetric and asymmetric compression contours show that peripherial gradients reduce the base pressure rise. Furthermore, relatively large changes in the near wake length scales and a slight reduction in

DD FORM 1 JAN 73 1473 EDITION OF 1 NOV 55 IS OBSOLETE

Unclassified

SECURITY CLASSIFICATION OF THIS PAGE (When Data Entered)

the base pressure occur when the solid-blockage effects of discrete radial fuel jets are modeled with pegs mounted near the base of the test projectile.

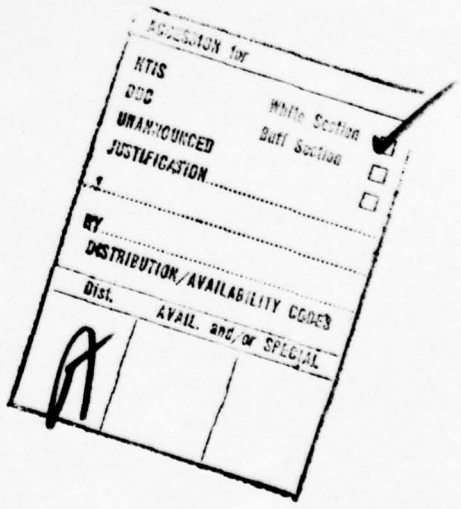

AFOSR Interim Scientific Report

AFOSR-TR-

Experiments and Analysis Related to External Burning for Propulsion

Prepared for

Air Force Office of Scientific Research
Aerospace Sciences Directorate
Bolling Air Force Base, D. C.

by

Douglas H. Neale
James E. Hubbartt
Warren C. Strahle
Walter W. Wilson

School of Aerospace Engineering
Georgia Institute of Technology
Atlanta, Georgia 30332

Approved for public release; distribution unlimited
Grant No. AFOSR 75-2794 March 1977

Abstract

An experimental study of base flows for a 2.25 inch diameter projectile at Mach 3 with and without simulated external burning disturbances is reported. Base pressure and wake structure results from systematic variations in axisymmetric external compression show that substantial base thrust can be produced and that the pressure and length scales of the external compression are imposed on the near wake. Measurements with comparable axisymmetric and asymmetric compression contours show that peripherial gradients reduce the base pressure rise. Furthermore, relatively large changes in the near wake length scales and a slight reduction in the base pressure occur when the solid-blockage effects of discrete radial fuel jets are modeled with pegs mounted near the base of the test projectile.

TABLE OF CONTENTS

I. INTRODUCTION

There are a great number of potential air-to-air, air-to-ground, and ground-to-air weaponry missions that require either a sustain or mild acceleration phase of the missile trajectory or which could benefit from substantial drag reduction during a portion of the trajectory. Furthermore, many of these missions require operation sufficiently low in the atmosphere that airbreathing propulsion, if it is competitive with the rocket, is attractive. Recent concepts of *external burning for propulsion* appear attractive for these missions because it is possible to make these systems extremely simple, essentially eliminating the requirement for an inlet, combustion chamber and nozzle with an acceptable sacrifice of I_{sp} compared to usual airbreathing systems. The feasibility of this concept, in which the subsonic near-wake transmits high downstream pressure to the base, has been experimentally established. An accurate theory to fully evaluate the potential of external burning has not yet, however, been proven. A major deficiency at the present time is the lack of detailed experimental data reflecting systematic alterations in the external flow field against which the theory can be tested. The present paper describes the results of the first phase of an experimental test program designed to provide proof that an analytical model currently under development will predict the effects on base pressure of many processes which take place during external burning.

II. TEST FACILITY

Flow System

The present base flow test facility was designed to simulate the base flow of a projectile at Mach 3 with a fineness ratio of about 6 and a Reynolds number, based on model diameter, in excess of 3.0×10^6. In addition, the facility design includes provisions for generating and exposing the base flow to disturbances simulating those expected with external burning for propulsion.

Figure 1 schematically shows the test facility flow system. The tunnel is a blow-down type with sufficient storage capacity at 3000 psig for up to 6 minutes of run time per charge depending on the desired test section stagnation pressure. Source air is reduced in pressure to about 350 psig by three parallel, remotely operated regulators with overlapping control ranges. Tunnel flow is accurately set with a hydraulically actuated, remote-controlled globe valve downstream of the main regulators. The flow is then passed through a large diameter plenum equipped with internal baffles and a perforated discharge plate to remove the gross non-uniformities introduced by throttling and turning. Final smoothing and straightening of the flow is achieved with a bell reducer and a combination of three screens and two honeycomb segments.

After the flow has been conditioned, it passes through a model support section, accelerates to Mach 3 in the nozzle and enters the transparent external compression section. This portion of the flow path is shown in more detail in Figure 2. The test section exhausts into a constant area shock diffuser for flow deceleration. An initial segment of the diffuser doubles as a support and guide through which pitot and static pressure probes can be

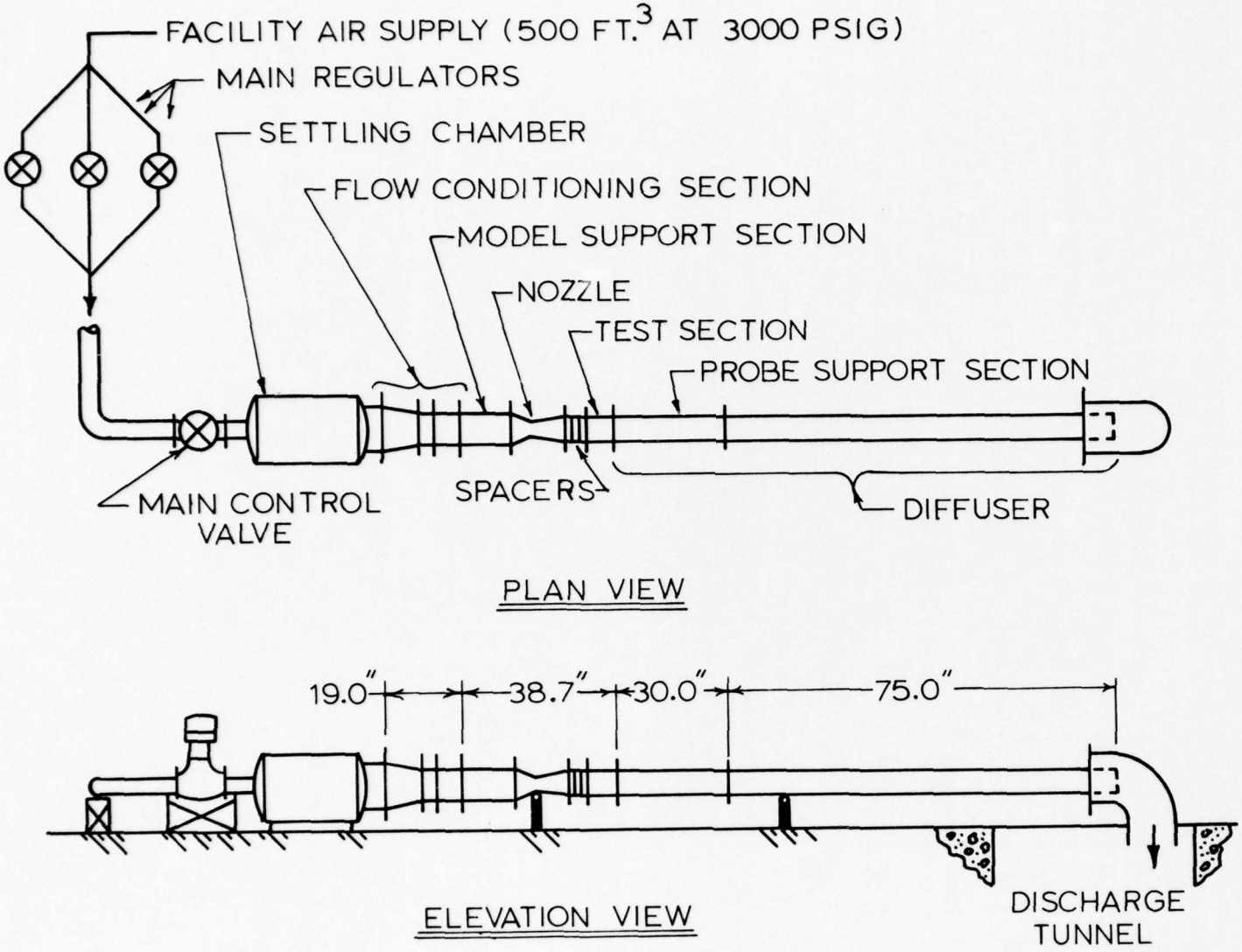

Figure 1. Base Flow Facility Schematic.

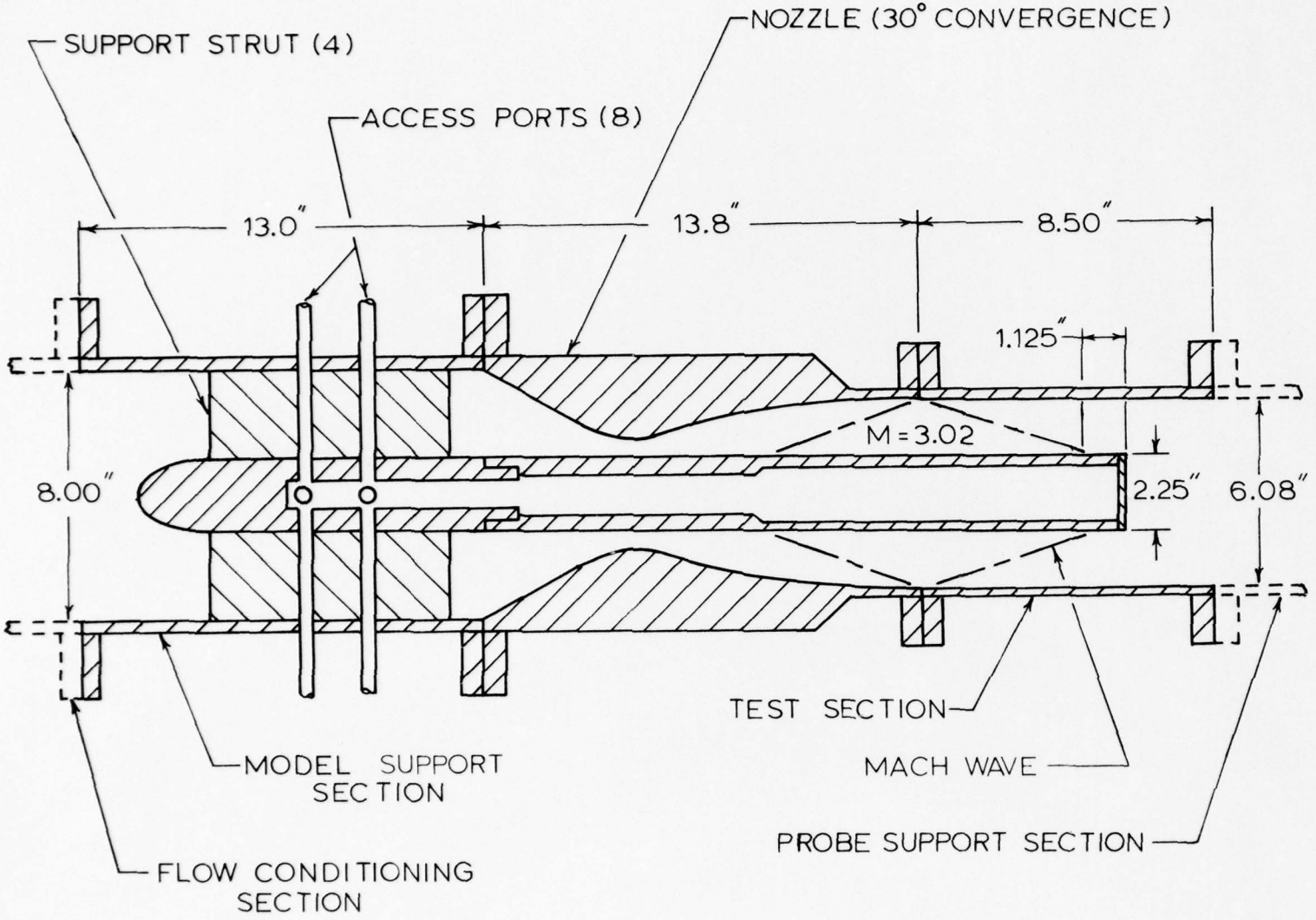

Figure 2. Base Flow Facility Test Section Detail.

introduced to the base flow region. After deceleration, the flow is dumped to atmosphere. Photographs of the base flow test facility are presented in Figure 3.

Instrumentation and Data Acquisition System

The current experimental configuration is instrumented with 56 surface static pressure taps: 7 on the model base, 16 on the model side walls, and 33 on the outer ducting from the nozzle exit to the diffuser discharge. Two thermocouples are bonded to the inner wall of the center-body model just upstream of the base and two additional thermocouples are imbedded in the nozzle wall near the exit plane. Static pressure and temperature data from the model are obtained by threading the respective leads forward through the centerbody bore and out access ports in the model mounting struts.

Total temperature and total pressure of the flow are measured with a thermocouple probe and a pitot probe located in the subsonic flow field just upstream of the model. The wake flow field is surveyed in two steps using separate telescoping pitot and static pressure probes. The wake region is surveyed with the probe traverse unit shown in the photographs of Figure 3. Two stepping motors provide accurate control of axial probe location in a vertical plane passing through the model center.

With the exception of upstream total pressure, measurement of pressures in base flow tests is done with two, 1000 mm Hg maximum pressure differential, variable capacitance type transducers. Each transducer is connected to a 48 port Scanivalve unit for rapid sampling of the pressure array. Upstream total pressure is measured with a strain gage transducer.

The data acquisition system is designed for manual control, used typically during test set-up, or for computer programmed operation employed during actual tests. A Hewlett-Packard 2100A computer with tape input and

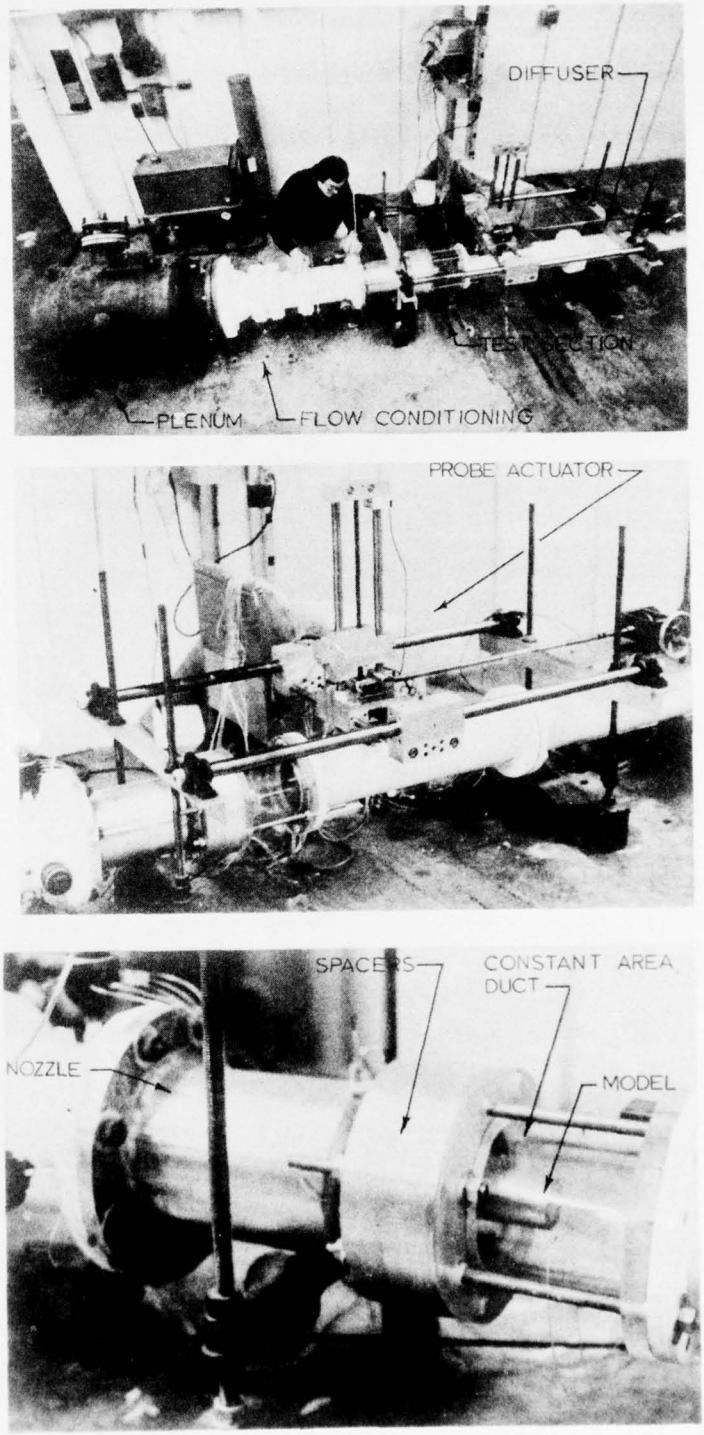

Figure 3. Base Flow Facility.

16K core storage capacity provides for system control, data acquisition, computation of flow parameters and final data output via teletype. Transducer voltage signals are received through a 30 channel scanner with a Hewlett-Packard 2401C low level, integrating digital voltmeter. The traverse stepper motors and scanivalve drivers are computer actuated through a multi-terminal relay card. The complete data system is shown schematically in Figure 4.

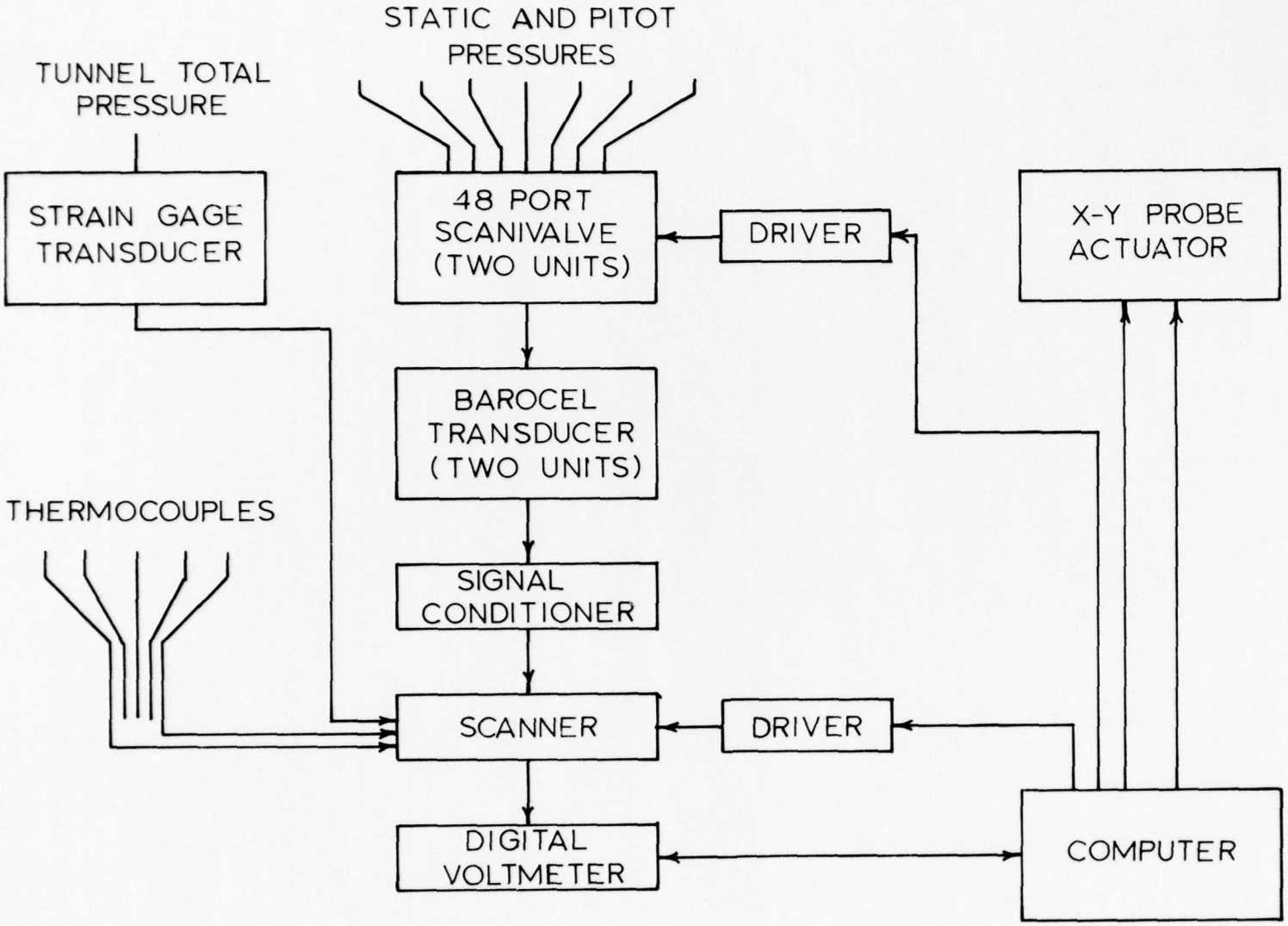

Figure 4. Base Flow Data Acquisition Schematic.

III. EXPERIMENTAL RESULTS

Initial Flow and Measurement Accuracy Evaluation

Before detailed base flow measurements were attempted, tests for flow field uniformity, data accuracy and repeatability and facility operation limits were performed. Calibration of the strain gage and variable capacitance transducers with a standard laboratory dead weight tester showed both devices to be highly linear. All transducers exhibited very slight shifts in calibration with time, on the order of months, and with repeated pressure cycling. Accordingly each transducer was checked periodically with the dead weight tester and current editions of the resulting calibration curves were inserted in the computer data retrieval programs. This procedure insured that absolute pressures were measured within $\pm$ 1% including wake and free stream static pressures that were typically less than 3 psia.

After pressure measurement accuracy was established, the tunnel flow field was evaluated using a constant-area test section duct matched to the nozzle exit diameter. A pitot survey of the flow conditioning section exit plane showed that variations in stagnation pressure among nozzle inlet streamlines was negligible in comparison with test section dynamic head. Flow quality was further verified with test section measurements yielding axial and peripheral Mach number distributions on the model and outer ducting surfaces. Mach numbers computed from test section measurements were found to be in close agreement with design values. As a typical example, the mean Mach number determined from four peripheral measurements on the model surface near the base plane was identical to the value of 2.98 conducted assuming one-dimensional flow corrected for theoretical boundary layer growth. Mean Mach number at this same plane computed from measurements

on the outer duct wall was 2.99. The mean values just described were computed from the results of six separate runs conducted on three days. The maximum deviation of any data point from the mean for this series of tests was found to be less than 1%. These base plane results coupled with similar results at other test section locations confirmed the ability of the apparatus to produce repeatable data.

Further diagnostic testing of the facility revealed minimum upstream stagnation pressures for proper diffuser performance in re-accelerating the subsonic wake to free stream velocities before shocking and discharging to atmosphere. In addition, surface temperature measurements showed that the model surface behaved virtually as an adiabatic wall so that heat transfer to the flow can be considered small. The effects of pressure lag due to transducer and line volumes were evaluated for the system and eliminated by establishing minimum scanning rates. Introduction of the static and pitot probes into the subsonic wake region was observed to have no discernable effect on base pressure. Finally, upstream stagnation pressure was varied over a range of reasonable operating conditions to check the Reynolds number effect on base pressure. For Reynolds numbers based on model diameter and free stream Mach number from 2.48×10^6 to 5.19×10^6 the differences in ratio of base pressure to upstream stagnation pressure were less than the stated accuracy of the data.

Zero External Disturbance Studies

An initial series of detailed wake measurements were performed using a constant-diameter test section to simulate base flow with no external disturbances other than those due to centerbody and outer duct boundary layers. The theoretical boundary layer momentum thickness on the model at the base plane was 1.2% of the model radius for a nominal test Reynolds number, based on centerbody diameter, of 2.7×10^6. Computation of the outer duct boundary layer at the nozzle exit showed similarly small characteristic dimensions.

Figures 5 and 6 present typical test measurements conducted in the near wake region. Figure 5 shows pitot and static pressure distributions along the model centerline downstream of the base. The corresponding centerline Mach number aft of the rear stagnation point is also displayed. P_1 and Po_1 denote the static and stagnation pressures in the free stream immediately ahead of the base plane. P and P_p are the probe-measured static and pitot pressures and M is the calculated Mach number. All pressures have been normalized by Po_1 measured almost simultaneously to minimize the effects of stagnation pressure drifts.

The rear stagnation point, determined from the intersection of the pitot and static pressure curves, is also specified in Figure 5. In addition, Figure 5 shows the smooth centerline flow acceleration from stagnation through sonic velocity. Finally, the ratio of static to stagnation pressure upstream of the base, P_1/Po_1, is included for comparison with the centerline static pressure distribution to illustrate the over-compression that occurs near the wake neck for axisymmetric base flow. This over-compression is primarily responsible for the higher base pressures demonstrated by axisymmetric bodies when compared with equivalent two-dimensional bodies.

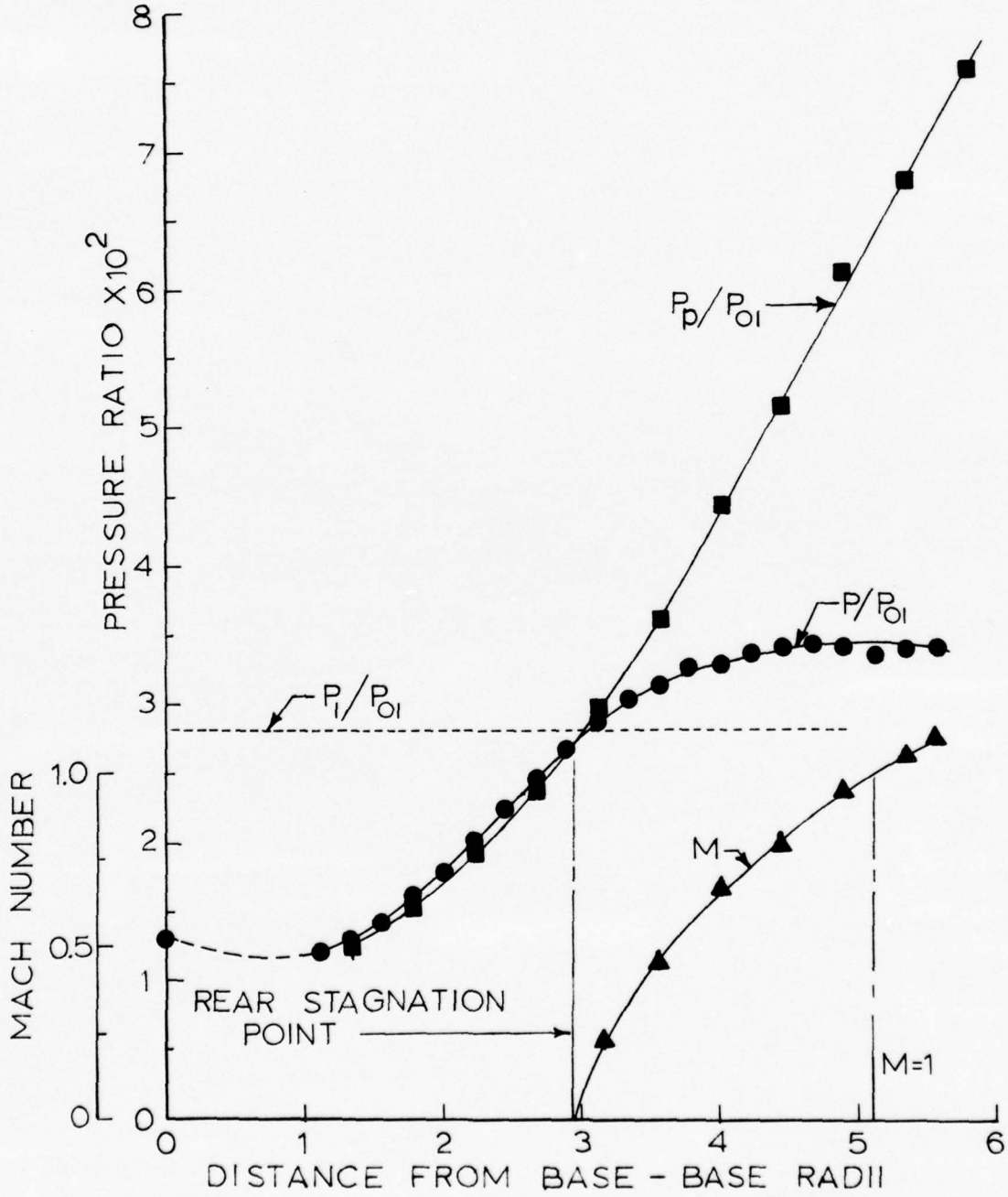

Figure 5. Near Wake Centerline Pressure and Mach Number Distributions - Constant Area Test Section (Zero External Compression).

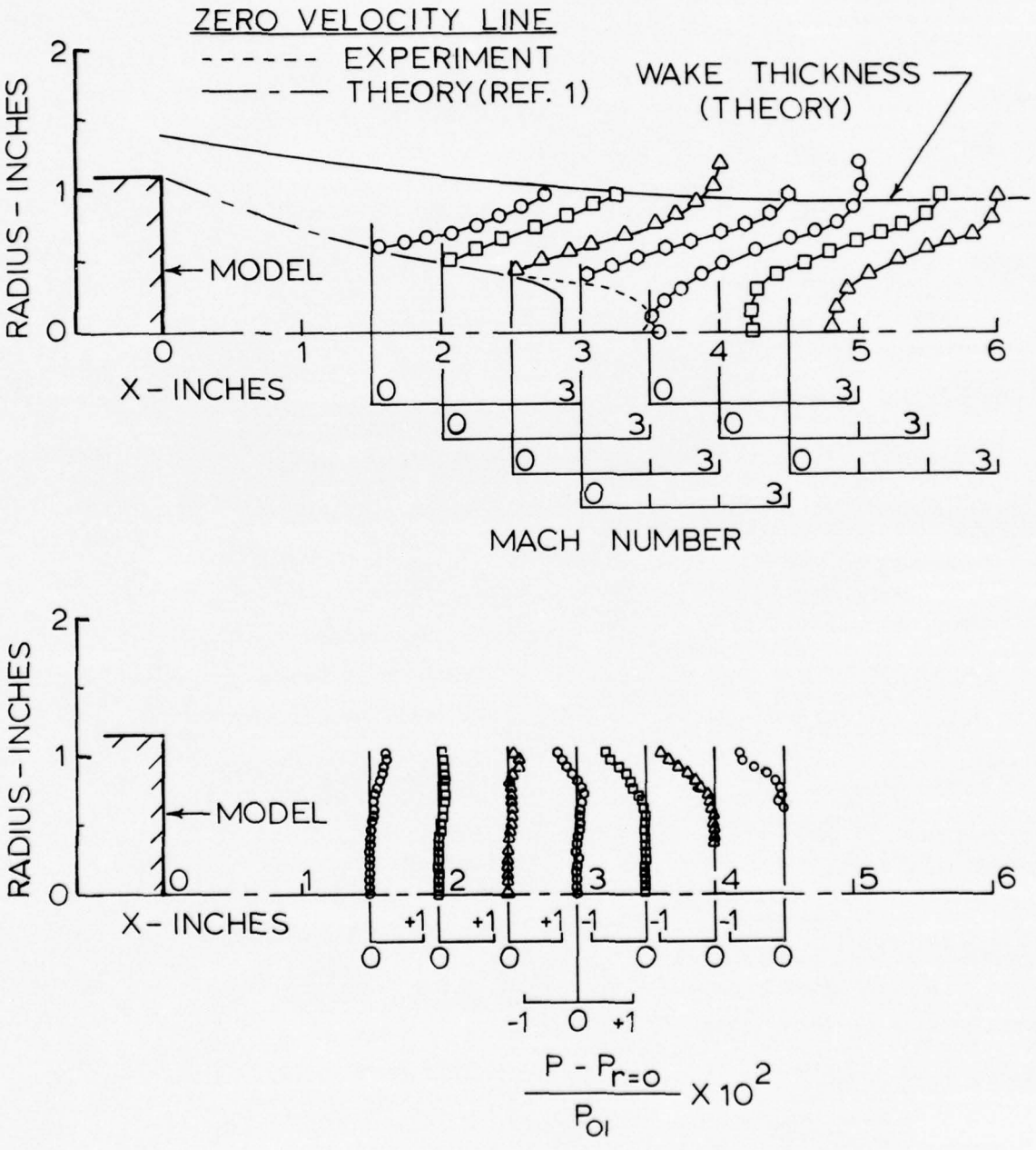

Figure 6. Near Wake Radial Mach Number and Static Pressure Distributions - Constant Area Test Section (Zero External Compression).

Figure 6. presents typical results from wake pitot and static pressure surveys in a vertical plane through the model centerline. Flow development in the wake outside of the recirculation region is shown by means of Mach number profiles in the upper portion of the figure. The experimental data is compared with a prediction of wake thickness and zero-velocity line position from a theory developed by Mehta and Strahle (Ref. 1). The theory is an integral method for solution of the fully turbulent, adiabatic near-wake field behind axisymmetric bluff base bodies in supersonic flow. Figure 6 shows excellent agreement between this theory and the experimentally determined wake thickness. The zero velocity line also matches well with experiment upstream of the theoretically predicted rear stagnation point.

The radial surveys reveal a slight assymmetry in the base flow which may suggest a minor redefinition of the rear stagnation point location. It was found that, in the vertical plane, the true wake centerline is displaced upwards such that a zero velocity point persists in the Mach number profile back to approximately 3.5 inches from the base. This represents a 0.2 inch axial shift in rear stagnation point from that determined by model centerline measurements. The true wake centerline offset at 3.5 inches from the base is 0.075 inches.

Radial static pressure surveys in the base flow region are shown in the lower portion of Figure 6. The variation from centerline pressure with increasing radius is consistent with streamline curvature as the flow initially converges toward and then turns back parallel with the axis. It should be noted that radial static pressure variations in the inner, lower velocity region of the shear flow are small when compared with the axial gradients.

Figures 7 and 8 compare the theory of Mehta and Strahle with the present experimental centerline results for static pressures in the near wake and for flow acceleration aft of the rear stagnation point (RSP). The slightly higher experimental base pressure in Figure 7 can be attributed to a small compression field

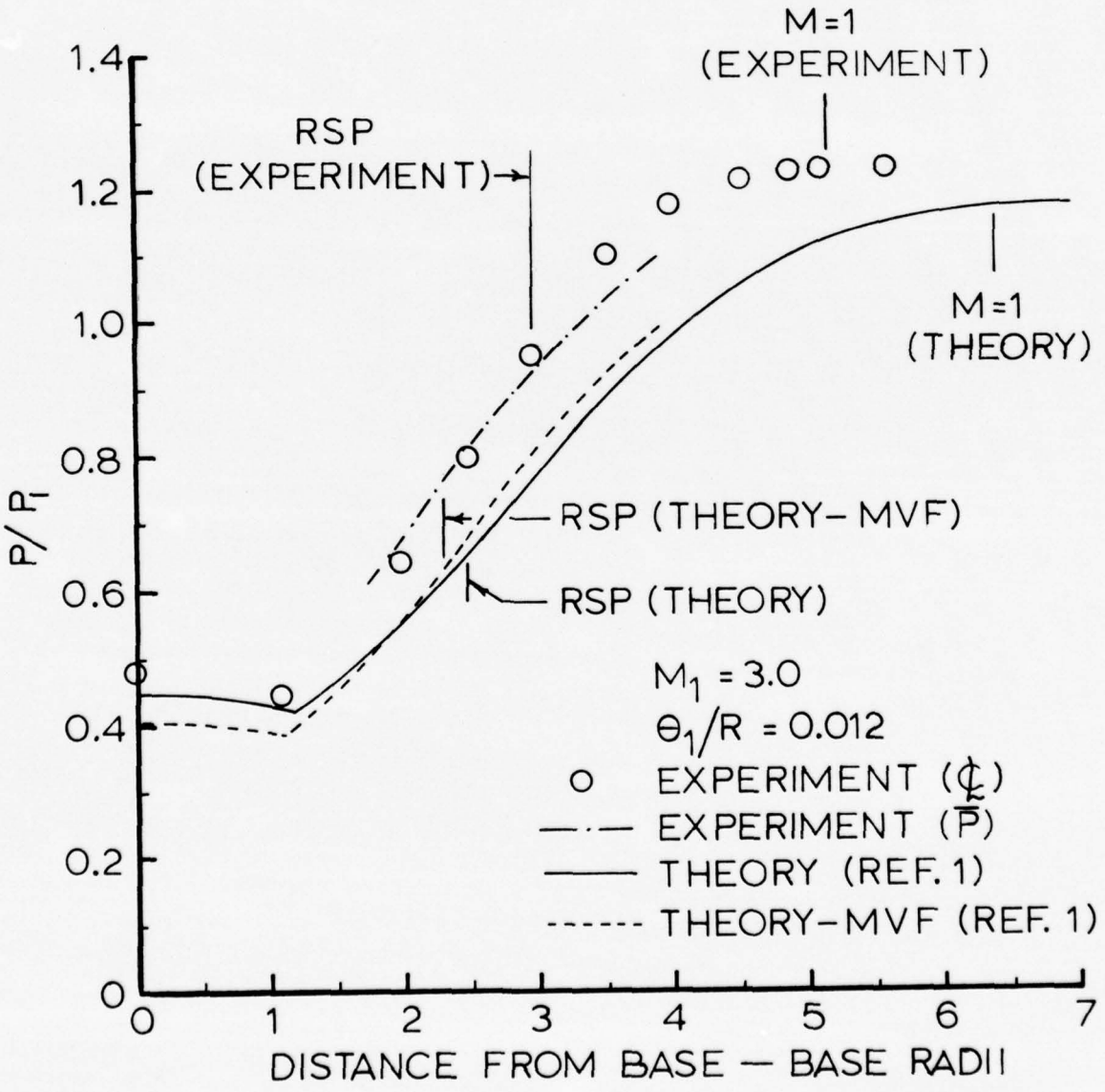

Figure 7. Comparison of Experimental Near Wake Centerline Static Pressure Distribution with Theoretical Prediction - Constant Area Test Section (Zero External Compression).

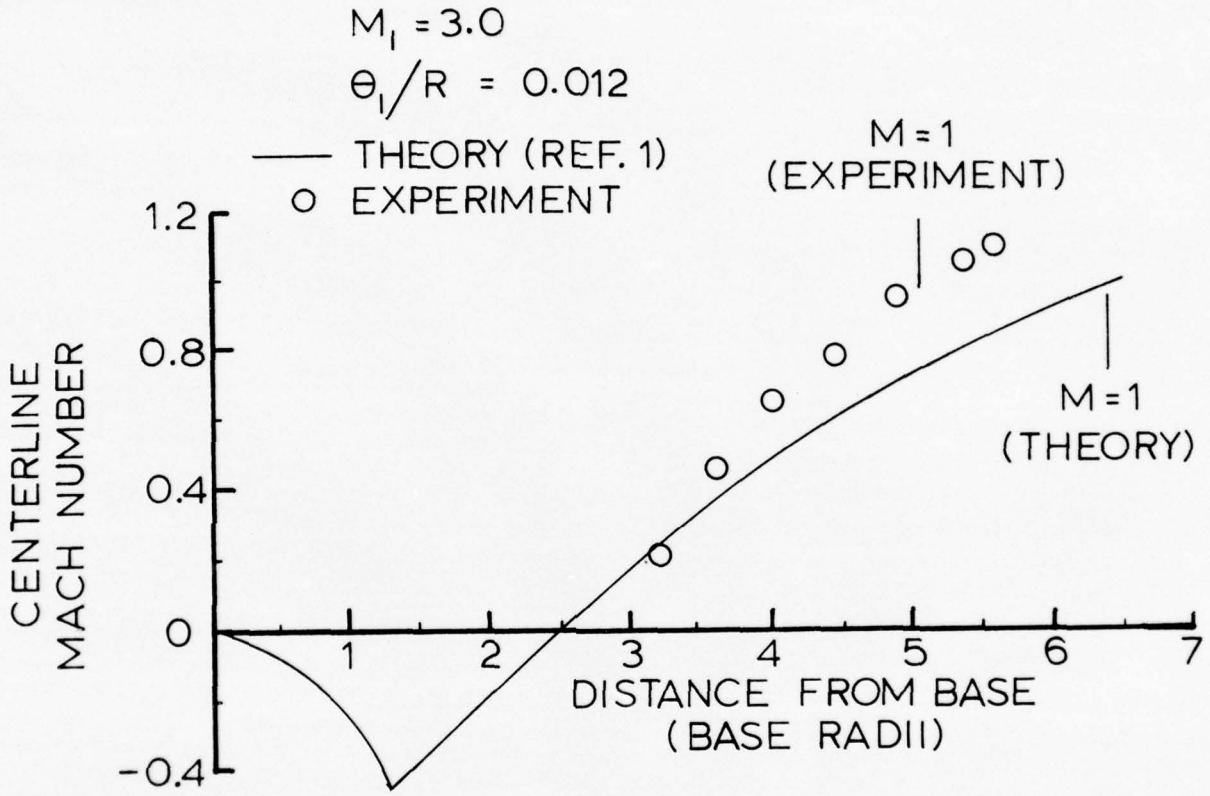

Figure 8. Comparison of Experimental Near Wake Centerline Mach Number Distribution with Theoretical Prediction - Constant Area Test Section (Zero External Compression).

initiated by the presence of a boundary layer on the outer duct. Both the experimental centerline static pressure data and a curve of the area-weighted mean static pressure, $\bar{P}$, have been included on the figure to show the small but significant effect of radial pressure gradients in the shear layer. The centerline static pressure distribution is predicted using two forms of the theory of Mehta and Strahle. The basic theory employs a standard compressible eddy viscosity model in the shear regions. Mehta and Strahle found, however, that a modified viscosity form (MVF) of the theory using an empirical initial free stream Mach number correction to the local eddy viscosity model yielded better correlation of experimental and theoretical results over a wider range of Mach numbers. In general, the analytical and experimental wake development shown in Figures 7 and 8 agree well.

Figure 9 compares similar solutions for incompressible axisymmetric wakes (Ref. 2) with two experimental velocity profiles. The experimental data radial coordinates are transformed to the incompressible form using a Stewartson-type transformation. These similar profiles and a set of nearly indistinguishable cosine profiles were both employed in the integral theory of Mehta and Strahle using a Stewartson-type transformation to account for compressibility. The experimental velocity profiles are in reasonably good agreement with the analytical representations. It is apparent that excellent agreement over the major portion of the profile would be obtained if the centerlines of the experimental data were shifted slightly so as to match experimental and analytical velocity gradients at the half-velocity point.

External Disturbance Studies

After completion of the base flow studies in an undisturbed free stream, the test facility was modified for simulation of external compression with burning. Replacement of the original constant area test section with a series of converging ducts provided free stream compression fields focused on the centerbody near

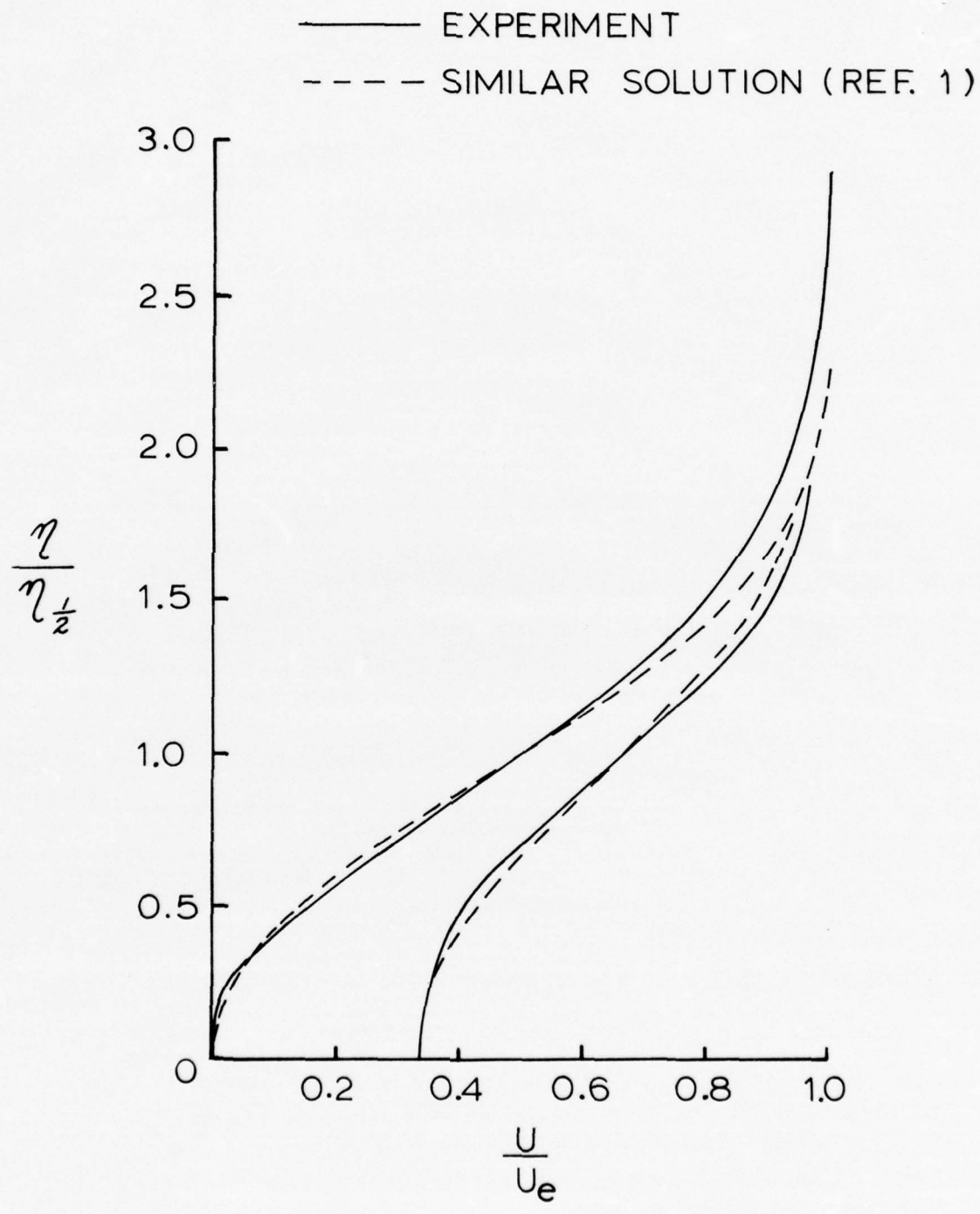

Figure 9. Comparison of Experimental and Similar Solution Velocity Profiles - Constant Area Test Section (Zero External Compression).

wake. The initial contour (Compression Section I) was designed to impose a pressure field on the wake that would approximately eliminate base drag. An axisymmetric heat released model was then constructed to duplicate the initial contour. Two subsequent alternate test section contours were then designed to simulate an identical total heat addition at varying release rates. A fourth test section was constructed using six symmetrically located half bodies of revolution attached to the inner wall of a cylindrical duct. The axial area distribution of this section was identical to that of the second axisymmetric compression section and was included to study the effects of equivalent heat addition in discrete plumes.

A series of five spacer rings were constructed to allow axial translation of the external disturbance ducts relative to the model. The inside diameter of the rings match the exit diameter of the nozzle and are inserted between the nozzle exhaust and the compression section inlet. Use of the spacers provides for translation of the external disturbance in increments of one base radius.

Finally, an alternate base plate was fabricated for modeling the solid body blockage of discrete radial fuel jets exhausting near the base. The jets were simulated with six solid cylindrical pegs fixed on the model perimeter to allow study of blockage effects without the complication of actual mass injection.

Axisymmetric Disturbance Test Results.

The design and performance of each axisymmetric compression duct are shown respectively in Figures 10 and 11. Figure 10 tabulates the axial distribution of design radius, Mach number and static pressure. Boundary layer growth has been accounted for in the Mach number and static pressure values. The design pressures are plotted in Figure 11 and are shown to be in good agreement with typical static pressure measurements on the duct surface.

The test configuration for external compression is shown in Figure 12 along with resulting base pressure measurements. The initial, mild contour (Compression section I) performed as designed by approximately eliminating base drag. A weak optimum axial location is shown for this case when the compression has been dis-

	COMPRESSION SECTION								
	I			II			III		
X IN.	R IN.	M	$P/P_{O_1} \times 10^2$	R IN.	M	$P/P_{O_1} \times 10^2$	R IN.	M	$P/P_{O_1} \times 10^2$
0	2.989	2.980	2.805	2.989	2.980	2.805	2.989	2.980	2.805
0.5	2.986	2.944	2.962	2.985	2.923	3.057	2.977	2.795	3.713
1	2.977	2.909	3.122	2.968	2.834	3.499	2.925	2.599	5.019
1.5	2.963	2.873	3.297	2.936	2.763	3.869	2.848	2.503	5.826
2	2.942	2.837	3.483	2.893	2.713	4.210	2.765	2.498	5.871
2.5	2.916	2.799	3.690	2.845	2.680	4.429	2.692	2.581	5.161
3	2.886	2.793	3.724	2.793	2.663	4.547	2.646	2.725	4.133
3.5	2.858	2.787	3.759	2.742	2.662	4.554	2.627	2.836	3.488
4	2.827	2.779	3.805	2.695	2.679	4.436	2.624	2.892	3.204
4.5	2.798	2.773	3.840	2.654	2.713	4.210	2.629	2.925	3.048
5	2.769	2.766	3.881	2.624	2.760	3.917	2.639	2.945	2.957
5.5	2.739	2.758	3.929	2.605	2.820	3.574			
6	2.710	2.749	3.984	2.600	2.883	3.248	2.666	2.965	2.869
6.5	2.681	2.749	3.984						
7	2.656	2.768	3.870	2.614	2.943	2.966	2.698	2.974	2.831
7.5	2.636	2.798	3.696						
8	2.625	2.829	3.525	2.644	2.965	2.869	2.733	2.977	2.818
8.5	2.621	2.867	3.328	2.662	2.969	2.852	2.751	2.977	2.818

Figure 10. Tabulation of Radius, Mach Number and Static Pressure Distributions for External Compression Test Section Ducts.

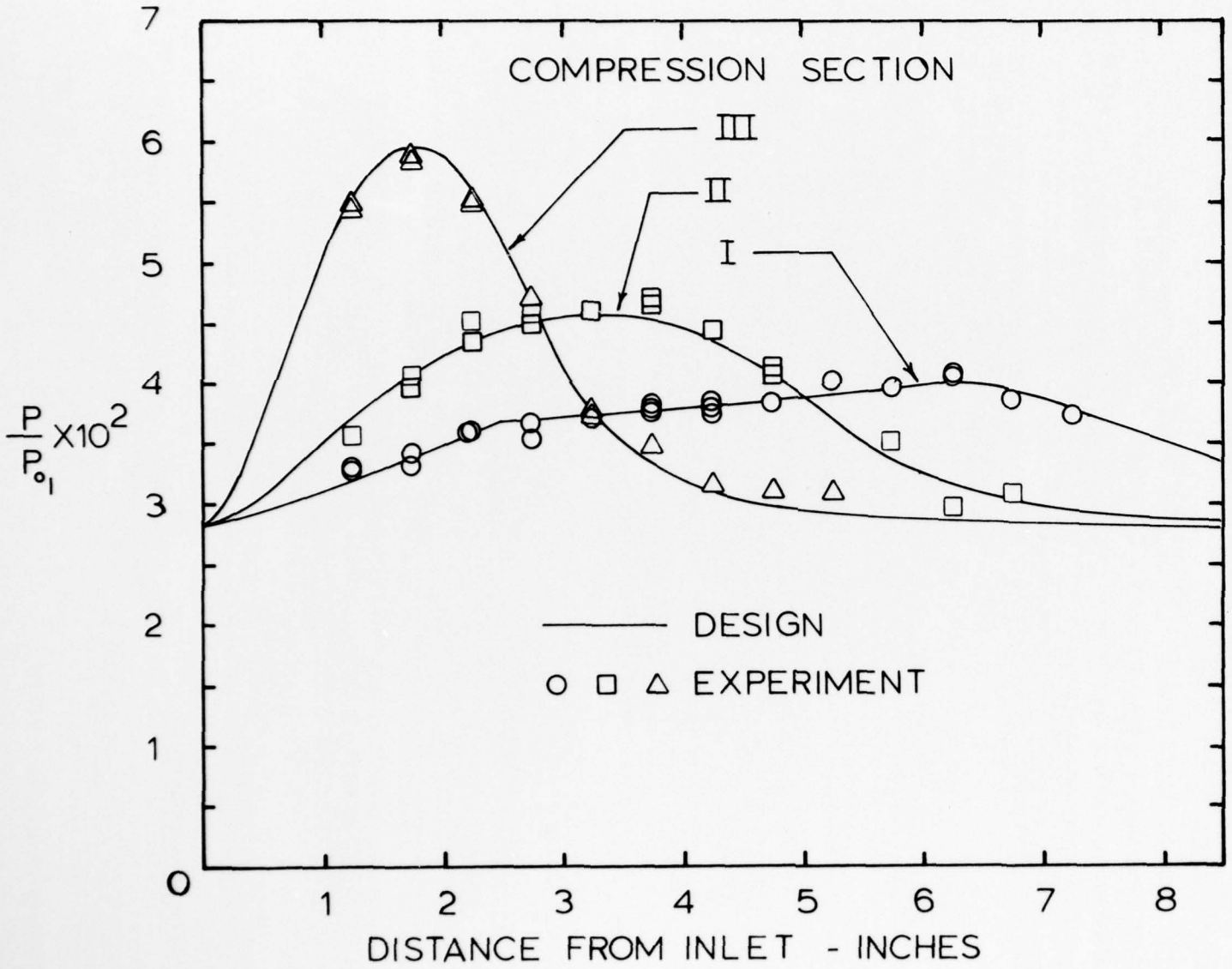

Figure 11. Comparison of External Compression Test Section Design and Performance.

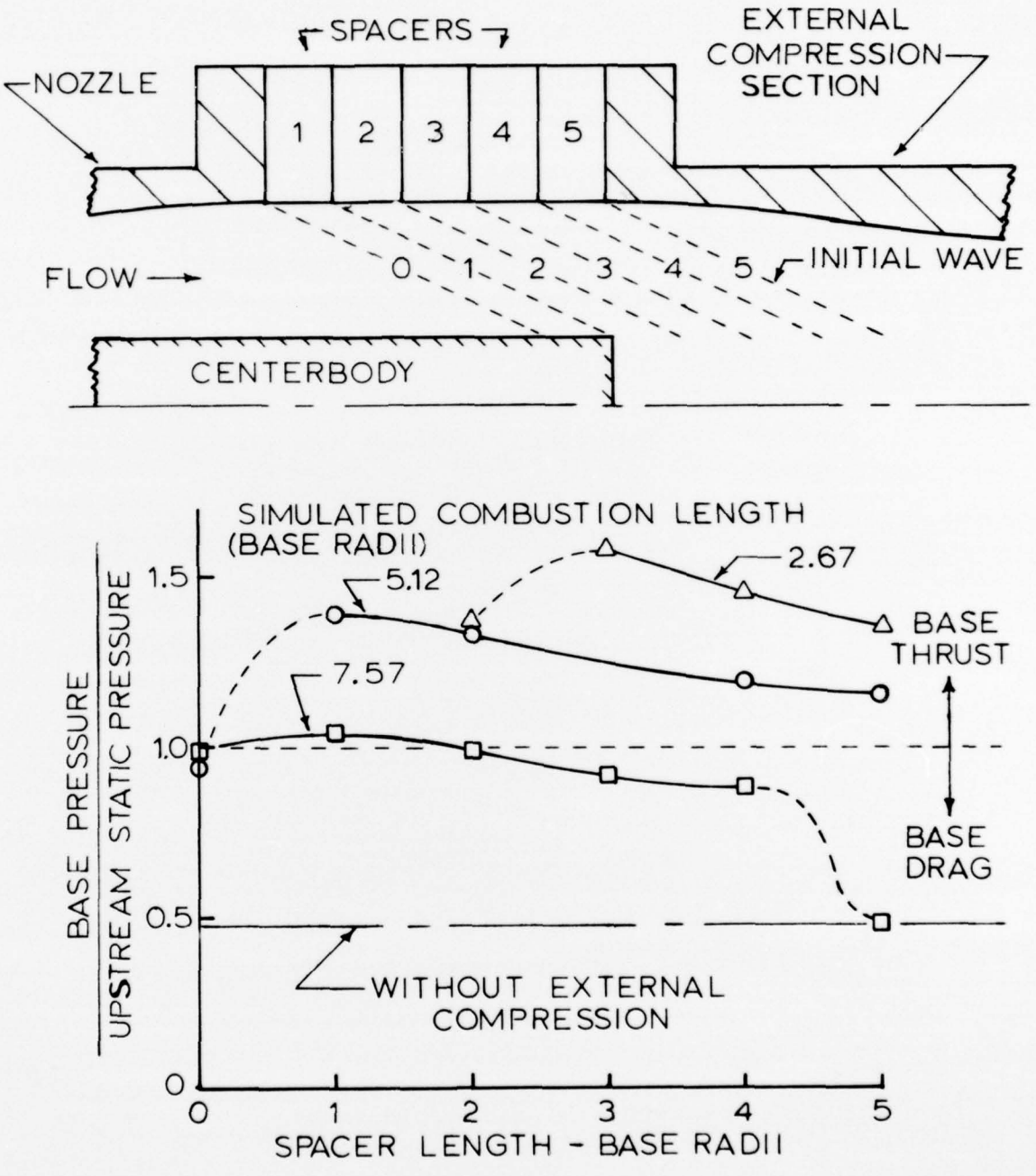

Figure 12. Effects of External Compression Strength and Location on Base Pressure.

placed downstream by one base radius. Base pressure falls slightly with the insertion of additional spacers up to a total of four. Base pressure, however, returns sharply to the value measured with a constant area duct when the fifth spacer is introduced. For this case, the initial compression wave intersects the wake downstream of the sonic point and can no longer influence the base region.

Translation of the two alternate axisymmetric disturbance sections verified the base flow trends shown with the original compression duct. As the compression severity increases, the optimum location of each duct moves downstream and the corresponding maximum base pressure rises. The rearward shift in optimum location probably results from the steepening of compression waves due to coalescence. Finally, Figure 12 shows that the third, most severe compression-rate duct yields an elevation in the base pressure sufficient to completely neutralize drag on a well designed projectile for which base and wave drag are typically comparable.

The systematic variation of disturbance position and strength revealed two additional characteristic lengths inherent in base flows with external compression. As shown in Figure 13, the wake length scales vary directly with location of the compression surfaces. Thus, movement of the disturbance field downstream tends to lengthen the distances from the base to the rear stagnation and sonic velocity points. Conversely, as the compression strength increases by decreasing the compression length for a fixed location, the wake length decreases.

Figure 14 further illustrates the direct relation of wake length to disturbance location for the initial, relatively mild compression surface. For those cases in which the compression field tends to elevate base pressure, the normalized centerline static pressure distributions clearly reflect disturbance loca-

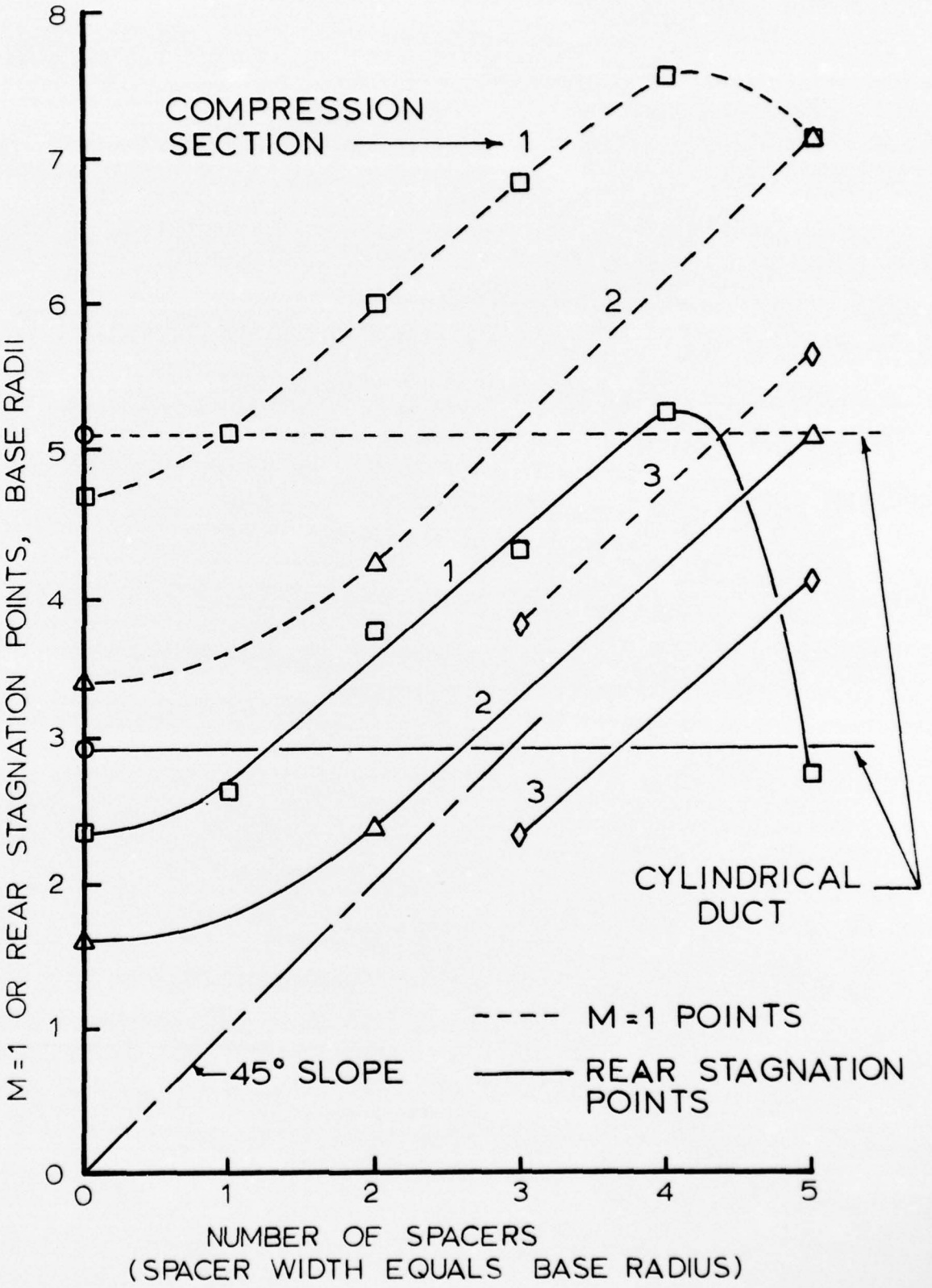

Figure 13. Effects of External Compression Strength and Location on Near Wake Length Scales.

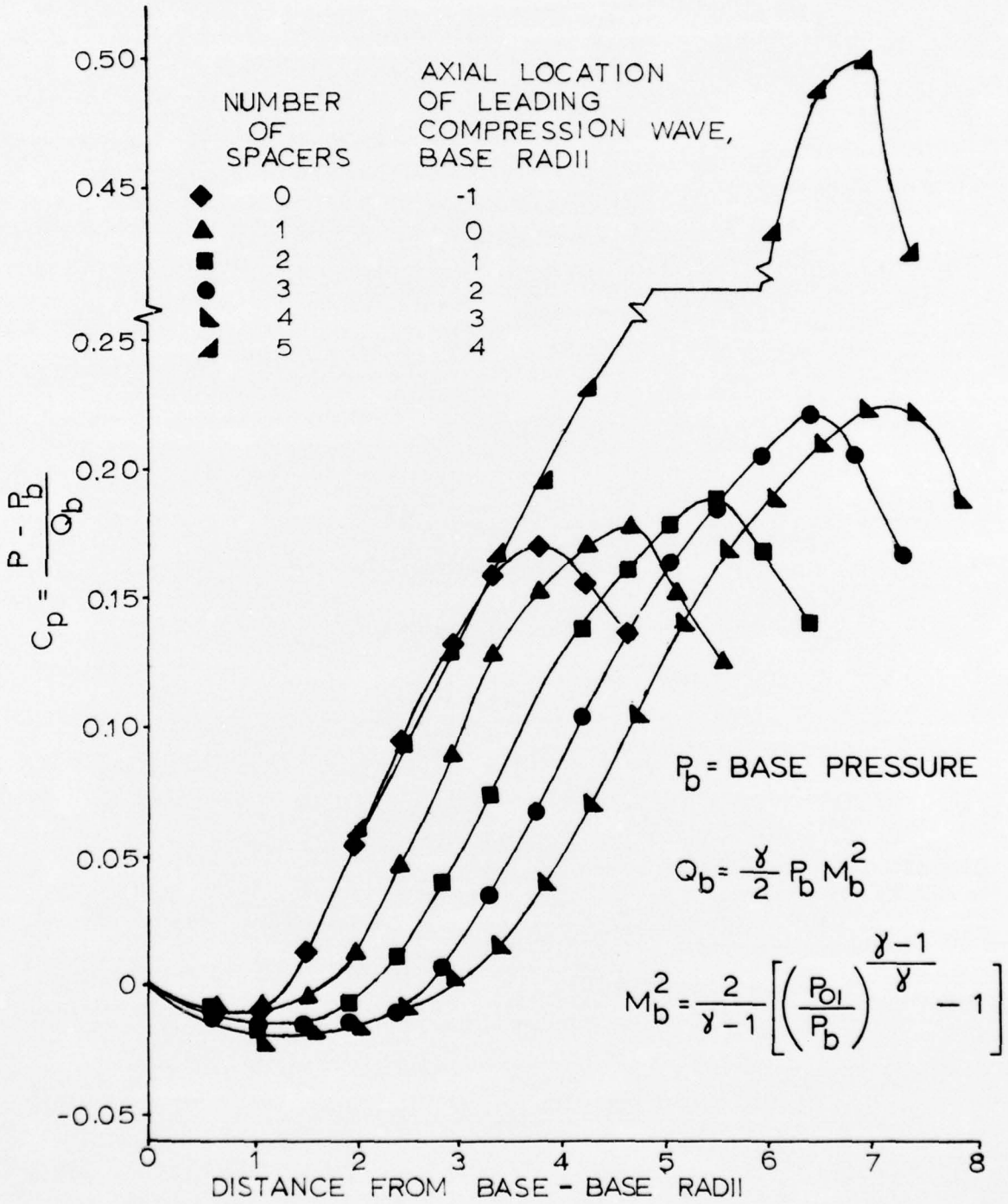

Figure 14. Effects of External Compression Location on Centerline Pressure Distribution - Compression Section I.

tion. The trend terminates abruptly, however, for the five-spacer case when base pressure reverts to the no-compression value.

Radial and axial measurements of Mach number and static pressure in the wake for the initial compression section with no spacers are shown in Figure 15. Comparison of the Mach number profiles for this case with those presented in Figure 6 for the cylindrical duct illustrates a slightly fuller and shortened recirculation region reflecting the elevated base pressure. As in Figure 6, the static pressure profiles in Figure 15 indicate the effects of flow curvature. In general, the radial pressure variation magnitudes are larger for the compression case resulting from the increased severity of turning associated with the shorter wake.

Discrete Disturbance Test Results.

In actual practice,external burning to influence base pressure would most likely take place in discrete plumes originating from radial fuel injection nozzles located near the projectile base. As mentioned previously, a fourth test section employing six half bodies of revolution was fabricated to compare the effects of discrete and equivalent axisymmetric disturbances. The axial area distribution of this fourth section was identical to that of the second compression duct (II).

Figure 16 schematically shows the fourth compression section along with base pressure test results for various axial duct locations. A significant reduction in base pressure from the axisymmetric case is seen at any given duct position. Figure 17 compares centerline static pressure and Mach number distributions for the axisymmetric and discrete distrubance ducts with two spacers. It is clear that, in addition to reducing base pressures, use of discrete disturbances has moved the rear stagnation point forward and has *midly increased the peak centerline static pressure.*

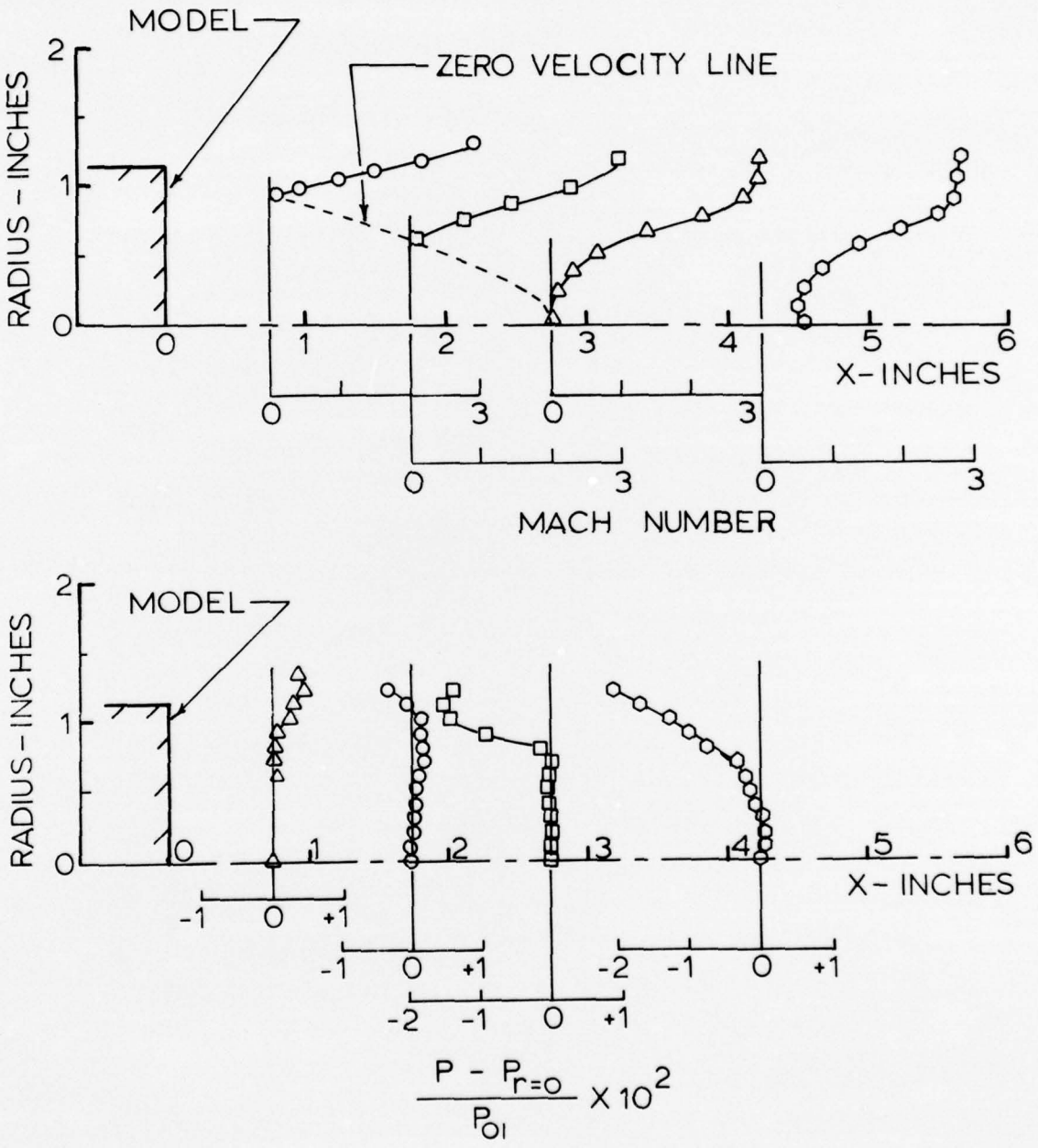

Figure 15. Near Wake Radial Mach Number and Static Pressure Distributions - Compression Section I, Zero Spacers.

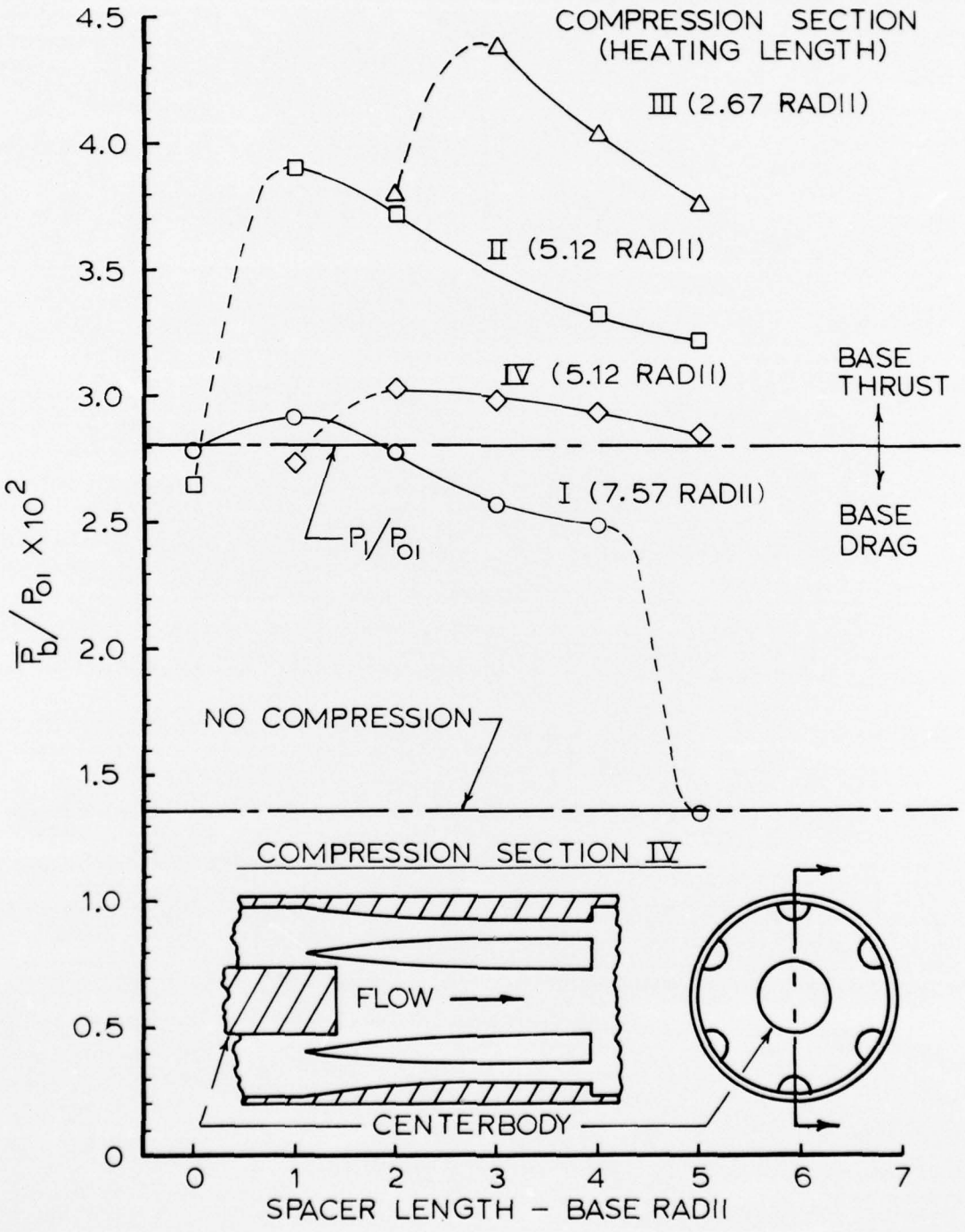

Figure 16. Comparison of Base Pressures for Axisymmetric and Equivalent Discrete Compression Sections (II and IV).

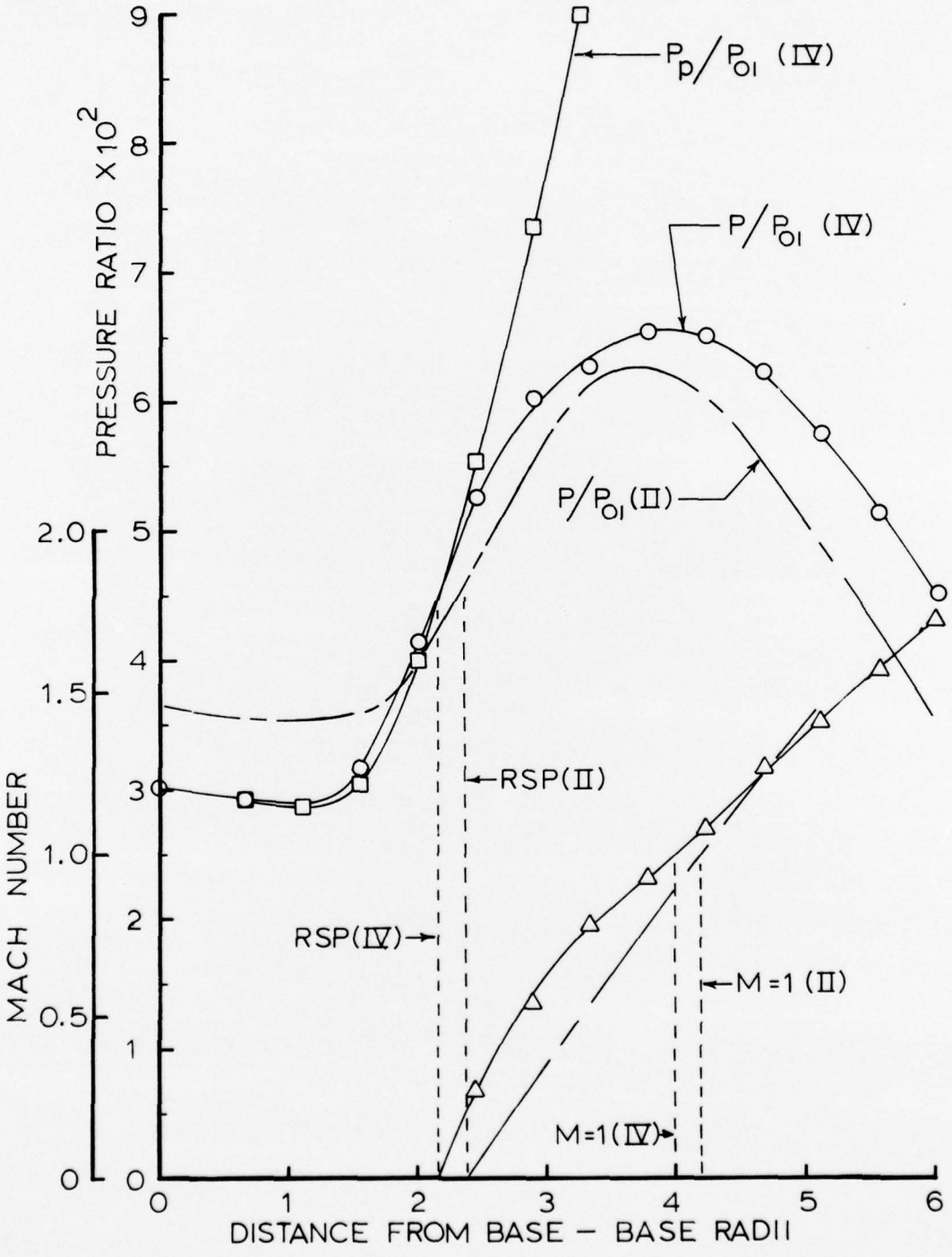

Figure 17. Comparison of Near Wake Centerline Pressure and Mach Number Distributions for Axisymmetric and Equivalent Discrete Compression Sections (II and IV).

It is believed that an explanation for the somewhat deteriorated performance just described may be found in a secondary vorticity field created by the discrete disturbance contours. Static pressure measurements along the duct and centerbody surfaces between half-bodies revealed considerably higher values than for the axisymmetric compression section (II). These higher wall pressures are due to coalescence of waves from adjacent contours and indicate the existence of strong peripheral pressure gradients in the free stream. Zones of higher pressure existing between half-bodies alternate with regions of lower pressure directly over the bodies and create the potential for streamwise secondary vorticity in the wake shear flow. The resulting increased mixing most certainly influences wake development by thickening and energizing the shear layer such as to increase its ability to oppose recompression. Since the maximum static pressure for the axisymmetric and discrete compression cases is nearly the same, base pressure for the discrete disturbance case must adjust downward to accommodate the increased pressure rise. It should be noted, however, that even though base pressure is lower for the discrete disturbance case, the base drag has still been neutralized.

To conclude the test program of simulating external burning disturbances without actual mass injection, the solid blockage of radial fuel jets exhausting near the base was modeled. For these tests an alternate base unit with six cylindrical pegs attached to the perimeter was substituted for the original base plate. The peg base is shown in Figure 18. The pegs were scaled to represent the solid body blockage associated with jets in crossflow excluding entrainment. Dimensions were based on the gaseous jet penetration analysis of Reference 3 assuming complete elimination of projectile drag with practical values of specific impulse and jet nozzle pressure ratio. Tests with the peg base model were conducted with the constant area (no compression) test section.

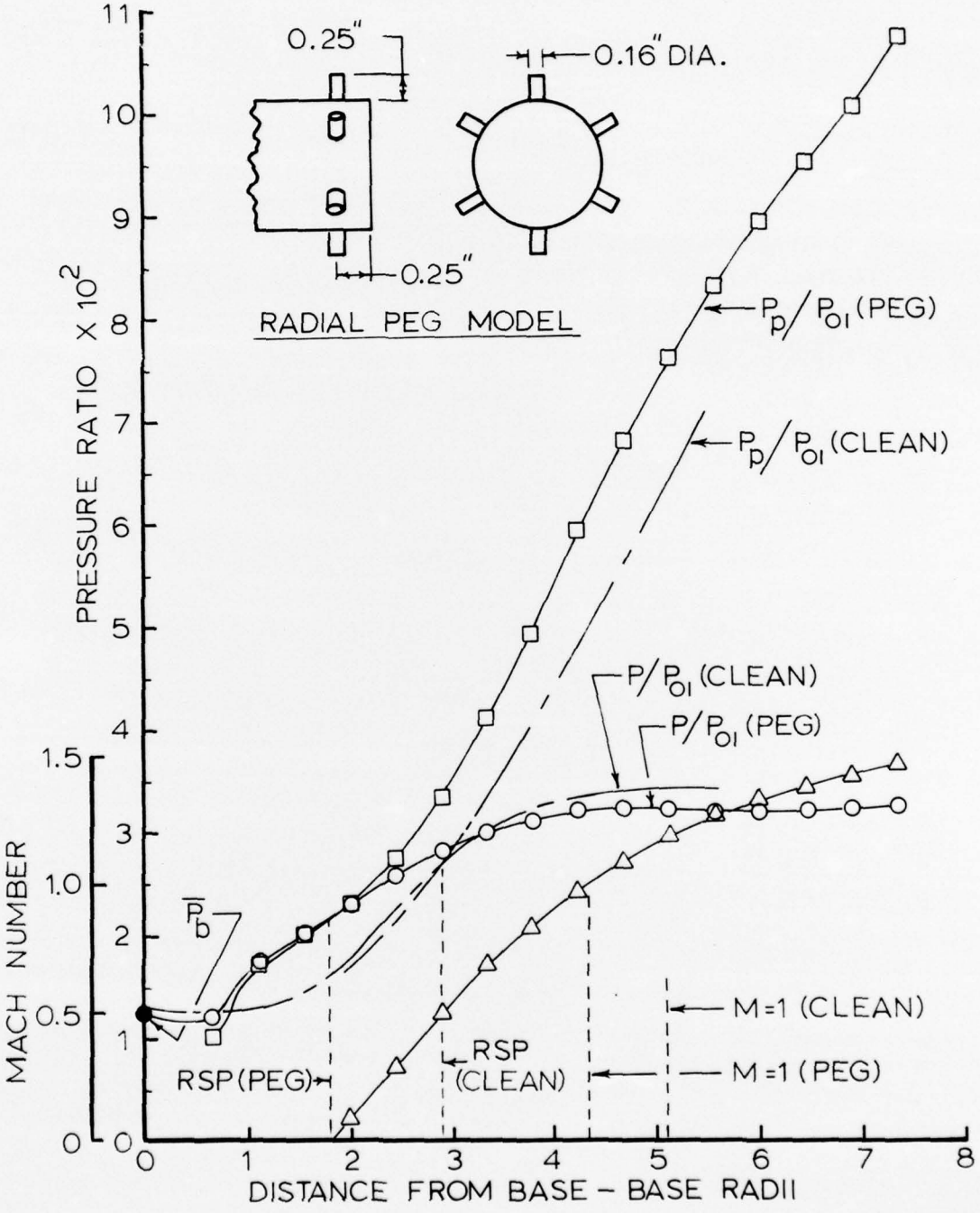

Figure 18. Comparison of Near Wake Centerline Pressure and Mach Number Distributions for Clean Base and Peg Base (Simulated Discrete Radial Jet Blockage).

Figure 18 presents the centerline pressure and Mach number distributions from the peg base tests. Results from the "clean" base tests are also provided to show changes in the wake structure. It is apparent that the presence of the pegs has significantly shortened the wake. Also, the base pressure, determined from a simple average of seven taps, is about 8% lower than the clean base configuration value of $\bar{P}_B/P_{o_1} = 1.36 \times 10^{-2}$. The reduction in the base pressure and the change in the base flow structure is thought to be primarily a result of increased mixing due to streamwise secondary vorticity generated by the pegs.

SUMMARY

The present experimental simulated external burning program has shown that substantial base thrust can be obtained by imposing axisymmetric or asymmetric compressions on the turbulent near-wake region of a projectile in supersonic flight. Systematic variations in disturbance strength and axial position reveal that the length scales of these compressions are reflected in the wake structure. As expected, base pressure rises and the near-wake shortens with increasing compression severity for any particular axial disturbance location. Downstream translation of a given disturbance acts to lengthen the wake and yields a mild optimum base pressure for that disturbance. The present tests demonstrate a case in which base pressure elevation is sufficient to completely neutralize base and forebody drag on a well designed projectile.

In actual practice, external burning will probably take place in discrete plumes originating from radial injection of fuel in the vicinity of the base plane. Tests simulating this configuration showed that base pressure elevation is significantly reduced for discrete externally generated disturbances when compared with the equivalent axisymmetric compression. The loss in base thrust is apparently related to streamwise vorticity created in and above the shear layer by the non-uniform external compression field. The present tests demonstrated, however, that base pressure had still been boosted sufficiently to eliminate base drag.

Finally, modeling of the solid body blockage effects of discrete radial fuel jets near the base showed relatively large changes in the near-wake length scales. Despite the alteration in wake structure, base pressure was only slightly lower than for a "clean" projectile with no radial jet modeling.

BIBLIOGRAPHY

Ref. 1. Mehta, G. K., and Strahle, W. C., "A Theory of the Supersonic Turbulent Axisymmetric Near Wake Behind Bluff-Base Bodies," to be published as AIAA Journal Synoptic.

Ref. 2. Kubota, T., Reeves, B. L., and Buss, H., "A Family of Similar Solutions for Axisymmetric Incompressible Wakes," AIAA Journal, 2, August 1964, pp. 1493-1495.

Ref. 3. Billig, F. S., Orth, R. C., and Lasky, M., "A Unified Analysis of Gaseous Jet Penetration," AIAA Journal, 9, June, 1971, pp. 1048-1058.